

Backward Monte Carlo Simulations in Radiative Heat Transfer

Michael F. Modest

e-mail: mfm6@psu.edu

Fellow ASME,

Department of Mechanical and Nuclear Engineering,

Penn State University,
University Park, PA 16802

Standard Monte Carlo methods trace photon bundles in a forward direction, and may become extremely inefficient when radiation onto a small spot and/or onto a small direction cone is desired. Backward tracing of photon bundles is known to alleviate this problem if the source of radiation is large, but may also fail if the radiation source is collimated and/or very small. In this paper various implementations of the backward Monte Carlo method are discussed, allowing efficient Monte Carlo simulations for problems with arbitrary radiation sources, including small collimated beams, point sources, etc., in media of arbitrary optical thickness. [DOI: 10.1115/1.1518491]

Keywords: Heat Transfer, Monte Carlo, Radiation, Scattering

Introduction

The “standard” Monte Carlo method for radiative heat transfer, as presented in various textbooks and review articles [1–3] is a “forward” method, i.e., a photon bundle is emitted and its progress is then followed until it is absorbed or until it leaves the system. The method can easily simulate problems of great complexity and, for the majority of problems where overall knowledge of the radiation field is desired, the method is reasonably efficient. However, if only the radiative intensity hitting a small spot and/or over a small range of solid angles is required, the method can become terribly inefficient. Consider, for example, a small detector (maybe $1\text{ mm} \times 1\text{ mm}$ in size) with a small field of view (capturing only photons hitting it from within a small cone of solid angles) monitoring the radiation from a large furnace filled with an absorbing, emitting and scattering medium. In a standard Monte Carlo simulation one would emit many photon bundles within the furnace, and would trace the path of each of these photons, even though only a very small fraction will hit the detector. It may take many billion bundles before a statistically meaningful result is achieved—at the same time calculating the intensity field everywhere (and without need): clearly a very wasteful procedure. Obviously, it would be much more desirable if one could just trace those photon bundles that eventually hit the detector.

This idea of a backward tracing solution, sometimes also known as *reverse Monte Carlo* has been applied by several investigators [4–10]. All of these investigations have been somewhat limited in scope, looking at light penetration through nonemitting oceans and atmospheres [4–6], computer graphics [7,8], reflecting boundaries [9], and emitting media [10]. All the aforementioned papers have dealt with large light sources (in volume and/or solid angle range), making a backward simulation straightforward. A number of other methods to overcome the inefficiency of standard Monte Carlo implementations in problems with small sources and/or detector have appeared in the Nuclear Engineering literature, e.g., [11–13].

It is the purpose of the present study to give a comprehensive formulation for backward Monte Carlo simulations in the area of radiative heat transfer, capable of treating emitting, absorbing and anisotropically scattering media, media with diffuse or collimated irradiation (with large or small footprints), media with point or line sources, etc. In addition, the method will be described in

terms of standard ray tracing (bundles of fixed energy) as well as using energy partition (bundles attenuated by absorption) [1] (also called “absorption suppression” by Walters and Buckius [3]).

Theoretical Development

Similar to the development of Walters and Buckius [10], we will start with the principle of reciprocity described by Case [14]. Let $I_{\lambda 1}$ and $I_{\lambda 2}$ be two different solutions to the radiative transfer equation for a specific medium,

$$\hat{\mathbf{s}} \cdot \nabla I_{\lambda j}(\mathbf{r}, \hat{\mathbf{s}}) = S_{\lambda j}(\mathbf{r}, \hat{\mathbf{s}}) - \beta_{\lambda}(\mathbf{r}) I_{\lambda j}(\mathbf{r}, \hat{\mathbf{s}}) + \frac{\sigma_{s\lambda}(\mathbf{r})}{4\pi} \int_{4\pi} I_{\lambda j}(\mathbf{r}, \hat{\mathbf{s}}') \Phi_{\lambda}(\mathbf{r}, \hat{\mathbf{s}}, \hat{\mathbf{s}}') d\Omega', \quad j=1,2, \quad (1)$$

subject to the boundary condition

$$I_{\lambda j}(\mathbf{r}_w, \hat{\mathbf{s}}) = I_{w\lambda j}(\mathbf{r}_w, \hat{\mathbf{s}}), \quad j=1,2, \quad (2)$$

where \mathbf{r} is a vector pointing to a location within the medium, $\hat{\mathbf{s}}$ is a unit direction vector at that point, S is the local radiative source, β is the extinction coefficient, σ_s the scattering coefficient, Φ is the scattering phase function, and Ω denotes solid angle. The principle of reciprocity states that these two solutions are related by the following identity:

$$\begin{aligned} & \int_A \int_{\hat{\mathbf{n}} \cdot \hat{\mathbf{s}} > 0} [I_{w\lambda 2}(\mathbf{r}_w, \hat{\mathbf{s}}) I_{\lambda 1}(\mathbf{r}_w, -\hat{\mathbf{s}}) \\ & - I_{w\lambda 1}(\mathbf{r}_w, \hat{\mathbf{s}}) I_{\lambda 2}(\mathbf{r}_w, -\hat{\mathbf{s}})] (\hat{\mathbf{n}} \cdot \hat{\mathbf{s}}) \delta\Omega dA \\ & = \int_V \int_{4\pi} [I_{\lambda 2}(\mathbf{r}, -\hat{\mathbf{s}}) S_{\lambda 1}(\mathbf{r}, \hat{\mathbf{s}}) - I_{\lambda 1}(\mathbf{r}, \hat{\mathbf{s}}) S_{\lambda 2}(\mathbf{r}, -\hat{\mathbf{s}})] d\Omega dV, \end{aligned} \quad (3)$$

where A and V denote integration over enclosure surface area and enclosure volume, respectively, and $\hat{\mathbf{n}} \cdot \hat{\mathbf{s}} > 0$ indicates that the integration is over the hemisphere on a point on the surface pointing into the medium.

In the Backward Monte Carlo scheme, the solution to $I_{\lambda 1}(\mathbf{r}, \hat{\mathbf{s}})$ [with specified internal source $S_{\lambda 1}(\mathbf{r}, \hat{\mathbf{s}})$ and boundary intensity $I_{w\lambda 1}(\mathbf{r}_w, \hat{\mathbf{s}})$] is found from the solution to a much simpler problem $I_{\lambda 2}(\mathbf{r}, \hat{\mathbf{s}})$. In particular, if we desire the solution to $I_{\lambda 1}$ at location \mathbf{r}_i (say, a detector at the wall) into direction $-\hat{\mathbf{s}}_i$ (pointing out of the medium into the surface), we choose $I_{\lambda 2}$ to be the

Contributed by the Heat Transfer Division for publication in the JOURNAL OF HEAT TRANSFER. Manuscript received by the Heat Transfer Division October 18, 2001; revision received June 10, 2002. Associate Editor: R. Skocypec.

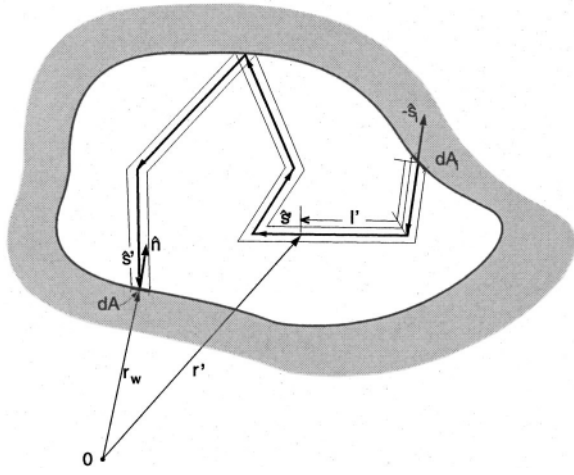


Fig. 1 Typical ray path in a backward Monte Carlo simulation

solution to a collimated point source of unit strength located also at \mathbf{r}_i , but pointing into the opposite direction, $+\hat{\mathbf{s}}_i$. Mathematically, this can be expressed as

$$I_{w\lambda 2}(\mathbf{r}_w, \hat{\mathbf{s}}) = 0, \quad (4a)$$

$$S_{\lambda 2}(\mathbf{r}, \hat{\mathbf{s}}) = \delta(\mathbf{r} - \mathbf{r}_i) \delta(\hat{\mathbf{s}} - \hat{\mathbf{s}}_i), \quad (4b)$$

where the δ are Dirac-delta functions for volume and solid angles, defined as

$$\delta(\mathbf{r} - \mathbf{r}_i) = \begin{cases} 0, & \mathbf{r} \neq \mathbf{r}_i, \\ \infty, & \mathbf{r} = \mathbf{r}_i, \end{cases} \quad (5a)$$

$$\int_V \delta(\mathbf{r} - \mathbf{r}_i) dV = 1, \quad (5b)$$

and similarly for solid angle. If the infinitesimal cross-section of the source, normal to $\hat{\mathbf{s}}_i$, is dA_i , then this results in an $I_{\lambda 2}$ intensity at \mathbf{r}_i of

$$I_{\lambda 2}(\mathbf{r}_i, \hat{\mathbf{s}}) = \frac{\delta(\hat{\mathbf{s}} - \hat{\mathbf{s}}_i)}{dA_i}. \quad (6)$$

As the $I_{\lambda 2}$ light beam travels through the absorbing and/or scattering medium, it will be attenuated accordingly.

Substituting Eqs. (4) into Eq. (3) yields the desired intensity as

$$I_{\lambda 1}(\mathbf{r}_i, -\hat{\mathbf{s}}_i) = \int_A \int_{\hat{\mathbf{n}} \cdot \hat{\mathbf{s}} > 0} I_{w\lambda 1}(\mathbf{r}_w, \hat{\mathbf{s}}) I_{\lambda 2}(\mathbf{r}_w, -\hat{\mathbf{s}}) (\hat{\mathbf{n}} \cdot \hat{\mathbf{s}}) d\Omega dA + \int_V \int_{4\pi} S_{\lambda 1}(\mathbf{r}, \hat{\mathbf{s}}) I_{\lambda 2}(\mathbf{r}, -\hat{\mathbf{s}}) d\Omega dV. \quad (7)$$

While the $I_{\lambda 2}$ problem is much simpler to solve than the $I_{\lambda 1}$ problem, it remains quite difficult if the medium scatters radiation, making a Monte Carlo solution desirable. Therefore, we will approximate $I_{\lambda 1}$ as the statistical average over N distinct paths that a photon bundle emitted at \mathbf{r}_i into direction $\hat{\mathbf{s}}_i$ traverses, as schematically shown in Fig. 1, or

$$I_{\lambda 1}(\mathbf{r}_i, -\hat{\mathbf{s}}_i) = \frac{1}{N} \sum_{n=1}^N I_{\lambda 1n}(\mathbf{r}_i, -\hat{\mathbf{s}}_i), \quad (8)$$

where the solution for each $I_{\lambda 1n}$ is found for its distinct statistical path (with absorption and scattering occurrences chosen exactly as in the forward Monte Carlo method). Along such a zig-zag path of total length l from \mathbf{r}_i to \mathbf{r}_w , consisting of several straight segments pointing along a local direction $\hat{\mathbf{s}}'(\mathbf{r}')$, $I_{\lambda 2}$ is nonzero only over an infinitesimal volume along the path, $dV = dA_i l$, and an infinitesimal solid angle centered around the local direction vector $-\hat{\mathbf{s}} = \hat{\mathbf{s}}'(\mathbf{r}')$. At its final destination on the enclosure surface, the beam of cross-section dA_i illuminates an area of only $dA = dA_i / (-\hat{\mathbf{s}}'(\mathbf{r}_w) \cdot \hat{\mathbf{n}})$, so that Eq. (7) simplifies to

tesimal solid angle centered around the local direction vector $-\hat{\mathbf{s}} = \hat{\mathbf{s}}'(\mathbf{r}')$. At its final destination on the enclosure surface, the beam of cross-section dA_i illuminates an area of only $dA = dA_i / (-\hat{\mathbf{s}}'(\mathbf{r}_w) \cdot \hat{\mathbf{n}})$, so that Eq. (7) simplifies to

$$I_{\lambda 1n}(\mathbf{r}_i, -\hat{\mathbf{s}}_i) = I_{w\lambda 1}(\mathbf{r}_w, -\hat{\mathbf{s}}'(\mathbf{r}_w)) \exp \left[- \int_0^l \kappa_\lambda(\mathbf{r}') dl' \right] + \int_0^l S_{\lambda 1}(\mathbf{r}', -\hat{\mathbf{s}}'(\mathbf{r}')) \exp \left[- \int_0^{l'} \kappa_\lambda(\mathbf{r}'') dl'' \right] dl', \quad (9)$$

where $\int_0^{l'} dl''$ indicates integration along the piecewise straight path, starting at \mathbf{r}_i , and κ_λ is the local absorption coefficient. It is seen that $I_{\lambda 1n}(\mathbf{r}_i, -\hat{\mathbf{s}}_i)$ consists of intensity emitted at the wall into the direction of $-\hat{\mathbf{s}}'(\mathbf{r}_w)$ (i.e., along the path toward \mathbf{r}_i), attenuated by absorption along the path, and by emission along the path due to the source $S_{\lambda 1}$, in the direction of $-\hat{\mathbf{s}}'(\mathbf{r}')$ (also along the path toward \mathbf{r}_i), and attenuated by absorption along the path, between the point of emission, \mathbf{r}' , and \mathbf{r}_i . This result is intuitively obvious since it is the same as the symbolic solution to the standard radiative transfer equation (RTE) [1], except that we here have a zig-zag path due to scattering and/or wall reflection events.

If we trace a photon bundle back toward its point of emission, allowing for intermediate reflections from the enclosure wall (as indicated in Fig. 1), then, at the emission point \mathbf{r}_w , $I_{w\lambda 1} = \epsilon_\lambda I_{b\lambda}(\mathbf{r}_w)$, where ϵ_λ is the local surface emittance (assumed to be diffuse here), and $I_{b\lambda}$ is the blackbody intensity or Planck function. And, if the internal source of radiation is due to isotropic emission, then, comparing the standard RTE [1] with Eq. (1) we find $S_{\lambda 1}(\mathbf{r}', -\hat{\mathbf{s}}') = \kappa_\lambda(\mathbf{r}') I_{b\lambda}(\mathbf{r}')$. Thus,

$$I_{\lambda n}(\mathbf{r}_i, -\hat{\mathbf{s}}_i) = \epsilon_\lambda(\mathbf{r}_w) I_{b\lambda}(\mathbf{r}_w) \exp \left[- \int_0^l \kappa_\lambda(\mathbf{r}') dl' \right] + \int_0^l \kappa_\lambda(\mathbf{r}') I_{b\lambda}(\mathbf{r}') \exp \left[- \int_0^{l'} \kappa_\lambda(\mathbf{r}'') dl'' \right] dl', \quad (10)$$

where the subscript “1” has been dropped since it is no longer needed. Equation (10) may be solved via a standard Monte Carlo simulation or using the energy partitioning scheme described by Modest [1] and Walters and Buckius [3]. For the standard method scattering lengths l_σ are chosen as well as an absorption length l_κ . The bundle is then traced backward from \mathbf{r}_i unattenuated [i.e., the exponential decay terms in Eq. (10) are dropped], until the total path length equals l_κ or until the emission location \mathbf{r}_w is reached (whichever comes first). Thus,

$$I_{\lambda n}(\mathbf{r}_i, -\hat{\mathbf{s}}_i) = \begin{cases} \int_0^{l_\kappa} \kappa_\lambda(\mathbf{r}') I_{b\lambda}(\mathbf{r}') dl', & l_\kappa < l, \\ \epsilon_\lambda(\mathbf{r}_w) I_{b\lambda}(\mathbf{r}_w) + \int_0^l \kappa_\lambda(\mathbf{r}') I_{b\lambda}(\mathbf{r}') dl', & l_\kappa \geq l \end{cases} \quad (11)$$

If energy partitioning is used only scattering lengths are chosen and $I_{\lambda n}$ is found directly from Eq. (10).

Radiative Fluxes. If radiative flux onto a surface at location \mathbf{r}_i over a finite range of solid angles is desired, the flux needs to be computed using the statistical data obtained for $I_{\lambda n}(\mathbf{r}_i, -\hat{\mathbf{s}}_i)$. For example, for a detector located at \mathbf{r}_i with opening angle θ_{\max} one obtains

$$\begin{aligned}
q_{\text{det}} &= \int_0^{2\pi} \int_0^{\theta_{\max}} \epsilon'_\lambda(\theta, \psi) I_{\lambda, \text{in}}(\theta, \psi) \cos \theta \sin \theta d\theta d\psi \\
&= \frac{1}{2} \int_0^{2\pi} \int_{\cos^2 \theta_{\max}}^1 \epsilon'_\lambda(\theta, \psi) I_{\lambda, \text{in}}(\theta, \psi) d(\cos^2 \theta) d\psi \\
&\approx \pi(1 - \cos^2 \theta_{\max}) \sum_{n=1}^N \epsilon'_\lambda(\hat{\mathbf{s}}_n) I_{\lambda, n}(-\hat{\mathbf{s}}_n), \quad (12)
\end{aligned}$$

where the directions $\hat{\mathbf{s}}_n$ need to be picked uniformly from the interval $0 \leq \psi \leq 2\pi$, $\cos^2 \theta_{\max} \leq \cos^2 \theta \leq 1$. The azimuthal angle ψ_n is found in standard fashion from $\psi_n = 2\pi R_\psi$, while θ_n is found from

$$\begin{aligned}
R_\theta &= \frac{\int_{\cos^2 \theta_{\max}}^1 d\zeta}{\int_{\cos^2 \theta_{\max}}^1 d\zeta} = \frac{1 - \cos^2 \theta_n}{1 - \cos^2 \theta_{\max}} = \frac{\sin^2 \theta_n}{\sin^2 \theta_{\max}}, \\
\text{or } \theta_n &= \sin^{-1}(\sqrt{R_\theta} \sin \theta_{\max}), \quad (13)
\end{aligned}$$

where R_θ and R_ψ are random numbers picked uniformly from $0 \leq R \leq 1$. If the detector is of finite dimension, points distributed across the surface are chosen like in a forward Monte Carlo simulation.

Collimated Irradiation. Backward Monte Carlo is extremely efficient if radiative fluxes onto a small surface and/or over a small solid angle range are needed. Conversely, forward Monte Carlo is most efficient if the radiation source is confined to a small volume and/or solid angle range. Both methods become extremely inefficient, or fail, if radiation from a small source intercepted by a small detector is needed. For collimated irradiation (and similar problems) backward Monte Carlo can be made efficient by separating intensity into a direct (collimated) and a scattered part, as outlined in Chapter 16 of [1]. Thus, letting $I(\mathbf{r}, \hat{\mathbf{s}}) = I_d(\mathbf{r}, \hat{\mathbf{s}}) + I_s(\mathbf{r}, \hat{\mathbf{s}})$, results in a direct component, attenuated by absorption and scattering,

$$I_d(\mathbf{r}, \hat{\mathbf{s}}) = q_{\text{coll}}(\mathbf{r}_w) \delta(\hat{\mathbf{s}} - \hat{\mathbf{s}}_0) \exp \left[- \int_{\mathbf{r} \rightarrow \mathbf{r}'} (\kappa + \sigma_s) ds' \right], \quad (14)$$

which satisfies the RTE without the inscattering term. This leads to a source term in the RTE for the scattered part of the intensity, due to (first) scattering of the collimated beam, of

$$S_{\lambda 1}(\mathbf{r}, \hat{\mathbf{s}}) = \sigma_s(\mathbf{r}) \frac{q_{\text{coll}}(\mathbf{r}_w)}{4\pi} \exp \left[- \int_0^{l_c} (\kappa_\lambda + \sigma_{s\lambda}) dl' \right] \Phi(\mathbf{r}, \hat{\mathbf{s}}_0, \hat{\mathbf{s}}), \quad (15)$$

where q_{coll} is the collimated flux entering the medium at \mathbf{r}_w , traveling a distance of l_c toward \mathbf{r} in the direction of $\hat{\mathbf{s}}_0$, and the scattering phase function $\Phi(\mathbf{r}, \hat{\mathbf{s}}_0, \hat{\mathbf{s}})$ indicates the amount of collimated flux arriving at \mathbf{r} from $\hat{\mathbf{s}}_0$, being scattered into the direction of $\hat{\mathbf{s}}$. Therefore, the diffuse component of the intensity at \mathbf{r}_i is found immediately from Eq. (9) as

$$I_{\lambda n}(\mathbf{r}_i, -\hat{\mathbf{s}}_i) = \int_0^l S_{\lambda 1}(\mathbf{r}', -\hat{\mathbf{s}}') \exp \left[- \int_0^{l'} \kappa_\lambda dl'' \right] dl', \quad (16)$$

with $S_{\lambda 1}$ from Eq. (15). As before, Eq. (16) may be solved using standard tracing [picking absorption length l_κ , and dropping the exponential attenuation term in Eq. (16)] or energy partitioning [using Eq. (16) as given].

Point and Line Source. Backward Monte Carlo also becomes inefficient if the radiation source comes from a very small surface or volume and/or if the source is unidirectional. The trick is again to break up intensity into a direct component (intensity coming directly from the source without scattering or wall reflect-

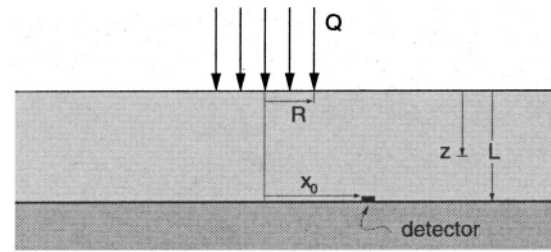


Fig. 2 One-dimensional slab with normally incident collimated irradiation

tions), and a multiply-scattered and reflected part. Again, we let I_d satisfy the radiative transfer equation without the inscattering term, or,

$$\hat{\mathbf{s}} \cdot \nabla I_d(\mathbf{r}, \hat{\mathbf{s}}) = S_d(\mathbf{r}, \hat{\mathbf{s}}) - \beta(\mathbf{r}) I_d(\mathbf{r}, \hat{\mathbf{s}}), \quad (17)$$

which has the simple solution

$$I_d(\mathbf{r}, \hat{\mathbf{s}}) = \int S_d(\mathbf{r}', \hat{\mathbf{s}}) \exp \left[- \int_{\mathbf{r} \rightarrow \mathbf{r}'} (\kappa + \sigma_s) ds' \right] ds, \quad (18)$$

where the main integral is along a straight path from the boundary of the medium to point \mathbf{r} in the direction of $\hat{\mathbf{s}}$. For example, if there is only a simple point source at \mathbf{r}_0 with total strength Q_0 , emitting isotropically across a tiny volume δV , Eq. (18) becomes

$$I_d(\mathbf{r}, \hat{\mathbf{s}}) = \frac{Q_0}{4\pi |\mathbf{r}_0 - \mathbf{r}|^2} \exp \left[- \int_{\mathbf{r}_0 \rightarrow \mathbf{r}} (\kappa + \sigma_s) ds' \right] \delta(\hat{\mathbf{s}} - \hat{\mathbf{s}}_0), \quad (19)$$

where $\hat{\mathbf{s}}$ is a unit vector pointing from \mathbf{r}_0 toward \mathbf{r} , and use has been made of the fact that

$$\delta V = \delta A \delta s = \frac{\delta \Omega_0 \delta s}{|\mathbf{r}_0 - \mathbf{r}|^2}, \quad (20)$$

where $\delta \Omega_0$ is the solid angle, with which δV is seen from \mathbf{r} . Equation (19) can be used to calculate the direct contribution of Q_0 hitting a detector, and it can be used to determine the source term for the RTE of the scattered radiation as

$$\begin{aligned}
S_1(\mathbf{r}, \hat{\mathbf{s}}) &= \frac{\sigma_s(\mathbf{r})}{4\pi} \int_{4\pi} I_d(\mathbf{r}, \hat{\mathbf{s}}') \Phi(\mathbf{r}, \hat{\mathbf{s}}', \hat{\mathbf{s}}) d\Omega' \\
&= \frac{\sigma_s(\mathbf{r}) Q_0}{16\pi^2 |\mathbf{r}_0 - \mathbf{r}|^2} \exp \left[- \int_{\mathbf{r}_0 \rightarrow \mathbf{r}} (\kappa + \sigma_s) ds' \right] \Phi(\mathbf{r}, \hat{\mathbf{s}}_0, \hat{\mathbf{s}}). \quad (21)
\end{aligned}$$

The rest of the solution proceeds as before, with $I_n(\mathbf{r}_i, -\hat{\mathbf{s}}_i)$ found from Eq. (16).

Sample Calculations

Isotropically Scattering, Nonabsorbing Medium With Collimated Irradiation. As a first example we will consider a one-dimensional slab $0 \leq z \leq L = 1$ m of a gray, purely isotropically scattering medium ($\sigma_s = 1 \text{ m}^{-1} = \text{const}$; $\Phi = 1$), bounded at the top ($z=0$) by vacuum and at the bottom ($z=L$) by a cold, black surface. Collimated irradiation of strength $Q = 100 \text{ W}$ is normally incident on this nonreflecting layer, equally distributed over the disk $0 \leq r \leq R = 0.1$ m, as shown in Fig. 2. A small detector $2 \text{ cm} \times 2 \text{ cm}$ in size, with an acceptance angle of θ_{\max} is located on the black surface at $x = x_0 = 0.2$ m, $y = 0$. The object is to determine the flux incident on the detector for varying acceptance angles, comparing forward and backward Monte Carlo implementations. In all simulations the number of photon bundles was doubled again and again until a relative variance of less than 2 percent of the desired quantity was achieved.

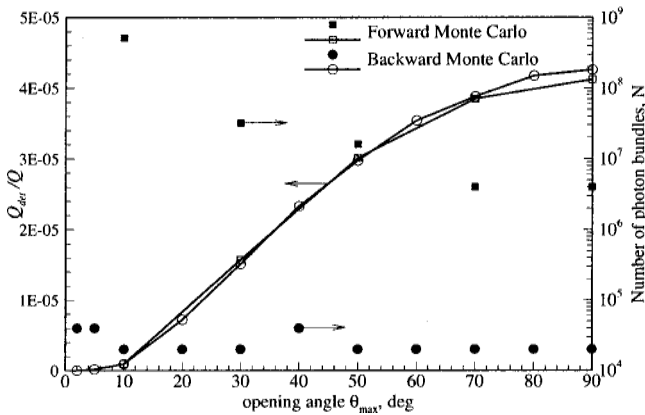


Fig. 3 Detector fluxes and required number of photon bundles (to achieve relative variance less than 2 percent) for one-dimensional slab with normally incident collimated irradiation

In a Forward Monte Carlo simulation emission points across the irradiation disk for N bundles are chosen, and emission is always into the $\hat{s}=\hat{k}$ or z -direction. Each bundle carries an amount of energy of Q/N and travels a distance of

$$l_\sigma = \frac{1}{\sigma_s} \ln \frac{1}{R_\sigma}, \quad (22)$$

before being scattered into a new direction, where R_σ is a random number picked uniformly from $0 \leq R_\sigma \leq 1$. For isotropic scattering the incident direction is irrelevant and one may set the new direction to that given for isotropic emission. The bundle is then traced along as many scattering paths as needed, until it leaves the layer ($z < 0$, or $z > L$). If the bundle strikes the bottom surface ($z = L$), incidence angle ($\hat{s} \cdot \hat{k} > \cos^2 \theta_{\max}$?) and location (x, y on detector?) are checked and a detector hit is recorded, if appropriate. Results are shown in Fig. 3. As the detector's acceptance angle increases, more photon bundles are captured. Obviously, this results in a larger detector-absorbed flux. However, it also increases the fraction of statistically meaningful samples, decreasing the variance of the results or the number of required photon bundles to achieve a given variance. Here all calculations were carried out until the variance fell below 2 percent of the calculated flux, and the necessary number of bundles is also included in the figure. For the chosen variance about 4×10^6 bundles are required for large acceptance angles, rising to 512×10^6 for $\theta_{\max} = 10$ deg. Results are difficult to obtain for $\theta_{\max} < 10$ deg. Similar remarks can be made for detector area: as the detector area decreases, the necessary number of bundles increases. Modeling a more typical detector $1 \text{ mm} \times 1 \text{ mm}$ in size would almost be impossible.

In a Backward Monte Carlo simulation, since no direct radiation hits the detector ($x_0 > R$), the scattered irradiation is calculated from Eqs. (16) and (15) with $q_{\text{coll}} = Q/\pi R^2$ as

$$I_n(\mathbf{r}_i, -\hat{s}_i) = \int_0^l \frac{\sigma_s Q}{4\pi^2 R^2} e^{-\sigma_s z} H(R - r(l')) dl', \quad (23)$$

where l consists of a number of straight-line segments, for which $dl' = dz'/\cos \theta$, and H is Heaviside's unit step function. Therefore,

$$\begin{aligned} I_n(\mathbf{r}_i, -\hat{s}_i) &= \frac{\sigma_s Q}{4\pi^2 R^2} \sum_j \int_{z_{1j}}^{z_{2j}} e^{-\sigma_s z} \frac{dz}{s_{zj}} \\ &= \frac{Q}{4\pi^2 R^2} \sum_j \frac{e^{-\sigma_s z_{1j}} - e^{-\sigma_s z_{2j}}}{s_{zj}}, \end{aligned} \quad (24)$$

where $s_{zj} = \cos \theta_j$ is the z -component of the direction vector for the j^{th} segment, and z_{1j} and z_{2j} are the z -locations between which

the segment lies within the cylindrical column $r \leq R$ (note that some segments may lie totally inside this column, some partially, and some not at all). Starting points distributed across the detector are chosen as in forward Monte Carlo, and a direction for the backward trace is picked from Eq. (13). Again, a scattering distance is found from Eq. (22), after which the bundle is scattered into a new direction. However, rather than having fixed energy, the backward-traveling bundles accumulate energy according to Eq. (24) as they travel through regions with a radiative source. The total flux hitting the detector is calculated by adding up bundle energies according to Eq. (12). Results are included in Fig. 3, and are seen to coincide with forward Monte Carlo results to about one variance or better (discrepancy being larger at large θ_{\max} , since the absolute variance increases). However, the number of required bundles remains essentially independent of opening angle at about 20,000 (and, similarly, independent of detector area). Since the tracing of a photon bundle requires essentially the same cpu time for forward and backward tracing, for the problem given here the backward Monte Carlo scheme is up to 25,000 times more efficient than forward Monte Carlo.

Absorbing/Scattering Medium With Collimated Irradiation.

Expanding on the previous example, for an acceptance angle of $\theta_{\max} = 10$ deg, we will now assume that the medium absorbs as well as scatters radiation, using absorption coefficients of $\kappa_\lambda = 1 \text{ m}^{-1}$ and $\kappa_\lambda = 5 \text{ m}^{-1}$. Forward as well as backward Monte Carlo will be used, and also both standard ray tracing as well as energy partitioning.

Forward Monte Carlo—Standard Ray Tracing. The solution proceeds as in the previous example, except that also an absorption length l_κ is chosen similar to Eq. (22). If the sum of all scattering paths exceeds l_κ , the bundle is terminated.

Forward Monte Carlo—Energy Partitioning. The solution proceeds as in the previous example, except the energy of each bundle hitting the detector is attenuated by a factor of $\exp(-\kappa l)$, where l is the total (scattered) path that the bundle travels through the layer before hitting the detector.

Backward Monte Carlo—Standard Ray Tracing. The solution proceeds as in the previous example, except for two changes. First, the local scattering source must be attenuated by absorption of the direct beam, and Eq. (24) becomes

$$\begin{aligned} I_n(\mathbf{r}_i, -\hat{s}_i) &= \frac{\sigma_s Q}{4\pi^2 R^2} \sum_j \int_{z_{1j}}^{z_{2j}} e^{-(\kappa + \sigma_s)z} \frac{dz}{s_{zj}} \\ &= \frac{\omega Q}{4\pi^2 R^2} \sum_j \frac{e^{-\beta z_{1j}} - e^{-\beta z_{2j}}}{s_{zj}}, \end{aligned} \quad (25)$$

where ω and β are scattering albedo and extinction coefficient, respectively. And again, an absorption length l_κ is chosen, and the addition in Eq. (25) is stopped as soon as the total path reaches l_κ or the bundle leaves the layer (which ever comes first).

Backward Monte Carlo—Energy Partitioning. Again, the scattering source must be attenuated as in Eq. (25), but the exponential attenuation term in Eq. (16) must also be retained. Thus,

$$I_n(\mathbf{r}_i, -\hat{s}_i) = \frac{\sigma_s Q}{4\pi^2 R^2} \int_0^l e^{-\beta z(l') - \kappa l'} H(R - r(l')) dl', \quad (26)$$

where the integrand contributes only where the source is active ($r \leq R$), but attenuation of the bundle takes place everywhere ($l' = \text{total distance along path from } \mathbf{r}_i \text{ to } \mathbf{r}'$). The rest of the simulation remains as in the previous case. Results are summarized in Table 1. As expected, if standard ray tracing is employed, the number of required bundles grows exponentially if the absorption coefficient becomes large, both for forward and backward Monte Carlo. While backward Monte Carlo retains its advantage (indeed, the forward Monte Carlo simulation for $\kappa_\lambda = 5 \text{ m}^{-1}$ could only be

Table 1 Comparison between four different Monte Carlo implementations to calculate irradiation onto a detector from a collimated source

κL	Forward MC— Standard		Forward MC— Energy partitioning		Backward MC— Standard		Backward MC— Energy partitioning	
	Q_{det}/Q	$N \times 10^{-6}$	Q_{det}/Q	$N \times 10^{-6}$	Q_{det}/Q	$N \times 10^{-6}$	Q_{det}/Q	$N \times 10^{-6}$
0	9.22×10^{-6}	512	9.22×10^{-6}	512	9.17×10^{-6}	0.02	9.17×10^{-6}	0.02
1	2.66×10^{-6}	512	2.70×10^{-6}	512	2.56×10^{-6}	0.08	2.59×10^{-6}	0.02
5	2.54×10^{-8}	16,384*	2.93×10^{-8}	512	2.77×10^{-8}	5.12	2.79×10^{-8}	0.02

*Variance of 5% (all other data have variance of 2%)

carried out to a variance of 5 percent), the relative growth of required bundles appears to be worse for backward Monte Carlo. If energy partitioning is employed, the number of bundles remains unaffected by the absorption coefficient for both, forward and backward Monte Carlo.

Isotropically Scattering, Nonabsorbing Medium With Internal Point Source. In a final example a point source of strength $Q_0 = 100$ W, located at $x_0 = y_0 = 0$, $z_0 = 0.5L$ will be considered for a purely scattering medium. Again, flux hitting the detector will be compared using forward and backward Monte Carlo methods.

The forward Monte Carlo simulation is almost identical to that of the first example, except that all photon bundles are now emitted from a single point, but into random directions. In the backward Monte Carlo simulation, the detector flux again consists of a direct and a scattered component and, again, the direct component is zero, this time because all direct radiation hits the detector at an angle larger than the acceptance angle. The I_n are then found from Eqs. (21) and (16) as

$$I_n(\mathbf{r}_i, -\hat{\mathbf{s}}_i) = \frac{\sigma_s Q}{16\pi^2} \sum_j \int_{l_{\sigma,j}} \frac{e^{-\sigma_s |\mathbf{r}_0 - \mathbf{r}|}}{|\mathbf{r}_0 - \mathbf{r}|^2} dl', \quad (27)$$

where the $l_{\sigma,j}$ are the straight paths the bundle travels between scattering events. Equation (27) must be integrated numerically, and this can be done using a simple Newton-Cotes scheme; here no optimization of the quadrature was attempted, except that—away from the source—the number of integration points was minimized for small l_{σ} (large σ_s). Alternatively, the integral can be obtained statistically from

$$I_n(\mathbf{r}_i, -\hat{\mathbf{s}}_i) = \frac{\sigma_s Q}{16\pi^2} \sum_j \frac{l_{\sigma,j}}{M} \sum_m \frac{e^{-\sigma_s |\mathbf{r}_0 - \mathbf{r}_m|}}{|\mathbf{r}_0 - \mathbf{r}_m|^2}, \quad (28)$$

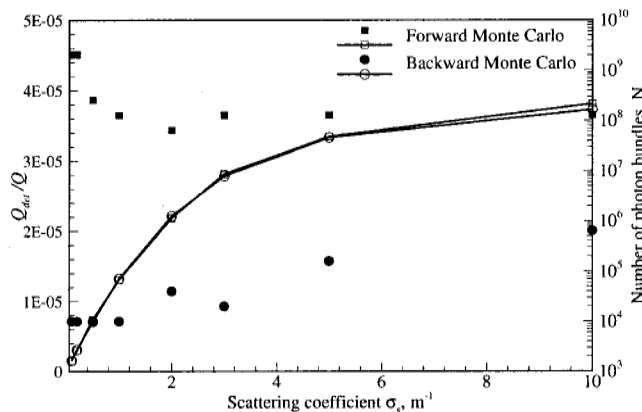


Fig. 4 Detector fluxes and required number of photon bundles (to achieve relative variance less than 2 percent) for one-dimensional slab with internal point source

where the \mathbf{r}_m are M random locations chosen uniformly along path $l_{\sigma,j}$. Results for detector flux as function of scattering coefficient are shown in Fig. 4.

For small values of σ_s the number of photon bundles required to achieve a relative variance of 2 percent is much smaller for the backward Monte Carlo method, as expected, since the volume with secondary scattering (i.e., the Source S_1) is relatively large, and the detector is small. However, as σ_s increases, the size of the secondary scattering volume decreases, and backward Monte Carlo becomes less and less efficient. For both methods large σ_s mean smaller $l_{\sigma,j}$, leading to increased tracing effort for each individual bundle. Numerical integration via Eq. (28) was generally much more efficient than Newton-Cotes quadrature, with $M = 1$ usually being sufficient (since the integral is evaluated so many times). However, for large σ_s this method became inefficient, requiring many photon bundles to achieve a 2 percent relative variance. In addition, all methods became inefficient for $\sigma_s > 10 \text{ m}^{-1}$.

Summary

A comprehensive formulation for backward Monte Carlo simulations, capable of treating emitting, absorbing and anisotropically scattering media, media with diffuse or collimated irradiation (with large or small footprints), media with point or line sources, etc., has been given. The basic backward Monte Carlo simulation of Walters and Buckius [3] was reviewed and was extended to allow for collimated irradiation, point sources, and other sources of small volume/area and/or small solid angle range. In addition, the method was extended to allow standard ray tracing (bundles of fixed energy) as well as energy partitioning (bundles attenuated by absorption). Sample results for radiation hitting a small detector show that forward Monte Carlo methods degrade rapidly with shrinking detector size and acceptance angle. Backward Monte Carlo, on the other hand, is unaffected by detector size, but requires a relatively large radiation source, which—in the case of collimated irradiation or point sources—needs to be created artificially by separating direct and scattered radiation. Even for relatively large detectors/opening angles, using backward Monte Carlo can result in several orders of magnitude lesser computer effort, and becomes the only feasible method for very small detectors. Similarly, using energy partitioning in strongly absorbing media also reduces numerical effort by orders of magnitude for, both, forward and backward Monte Carlo simulations.

Nomenclature

- A = area, m^2
- I = radiative intensity, $\text{W}/\text{m}^2 \text{sr}$
- l = geometric length, m
- $\hat{\mathbf{n}}$ = unit surface normal
- N = number of photon bundles
- q = radiative heat flux, W/m^2
- \mathbf{r} = position vector
- R = random number
- $\hat{\mathbf{s}}$ = unit direction vector
- S = radiative source, $\text{W}/\text{m}^3 \text{sr}$

T = temperature, K

V = Volume, m^3

Greek Symbols

β = extinction coefficient, cm^{-1}

ϵ = surface emittance

λ = wavelength, μm

Φ = scattering phase function

κ = absorption coefficient, cm^{-1}

Ω = solid angle, sr

σ_s = scattering coefficient, cm^{-1}

θ, ψ = incidence angles, rad

Subscripts

b = blackbody emission

j = path identifier

n = bundle identifier

w = wall

λ = spectral

References

- [1] Modest, M. F., 1993, *Radiative Heat Transfer*, McGraw-Hill, New York.
- [2] Siegel, R., and Howell, J. R., 1992, *Thermal Radiation Heat Transfer*, 3rd ed., Hemisphere, New York.
- [3] Walters, D. V., and Buckius, R. O., 1992, "Monte Carlo Methods for Radiative Heat Transfer in Scattering Media," in *Annual Review of Heat Transfer*, **5**, Hemisphere, New York, pp. 131–176.
- [4] Gordon, H. R., 1985, "Ship Perturbation of Irradiance Measurements at Sea: 1—Monte Carlo Simulations," *Appl. Opt.*, **24**, pp. 4172–4182.
- [5] Collins, D. G., Blättner, W. G., Wells, M. B., and Horak, H. G., 1972, "Backward Monte Carlo Calculations of the Polarization Characteristics of the Radiation Emerging From Spherical-Shell Atmospheres," *Appl. Opt.*, **11**, pp. 2684–2696.
- [6] Adams, C. N., and Kattawar, G. W., 1978, "Radiative Transfer in Spherical Shell Atmospheres—I. Rayleigh Scattering," *Icarus*, **35**, pp. 139–151.
- [7] Nishita, T., Miyawaki, Y., and Nakamae, E., 1987, "A Shading Model for Atmospheric Scattering Considering Luminous Intensity Distribution of Light Sources," *Comput. Graph.*, **21**, pp. 303–310.
- [8] Sabella, P., 1988, "A Rendering Algorithm for Visualizing 3D Scalar Fields," *Comput. Graph.*, **22**, pp. 51–58.
- [9] Edwards, D. K., 1983, "Numerical Methods in Radiation Heat Transfer," in *Proc. Second National Symposium on Numerical Properties and Methodologies in Heat Transfer*, Shih, T. M., ed., Hemisphere, pp. 479–496.
- [10] Walters, D. V., and Buckius, R. O., 1992, "Rigorous Development For Radiation Heat Transfer In Nonhomogeneous Absorbing, Emitting And Scattering Media," *Int. J. Heat Mass Transf.*, **35**, pp. 3323–3333.
- [11] Cramer, S. N., 1996, "Forward-Adjoint Monte Carlo Coupling With No Statistical Error Propagation," *Nucl. Sci. Eng.*, **124**(3), pp. 398–416.
- [12] Serov, I. V., John, T. M., and Hoogenboom, J. E., 1999, "A Midway Forward-Adjoint Coupling Method for Neutron and Photon Monte Carlo Transport," *Nucl. Sci. Eng.*, **133**(1), pp. 55–72.
- [13] Ueki, T., and Hoogenboom, J. E., 2001, "Exact Monte Carlo Perturbation Analysis by Forward-Adjoint Coupling in Radiation Transport Calculations," *J. Comput. Phys.*, **171**(2), pp. 509–533.
- [14] Case, K. M., 1957, "Transfer Problems and the Reciprocity Principle," *Rev. Mod. Phys.*, **29**, pp. 651–663.